WL-TR-97-1192

Bragg Cell on TeO_2 for 2-D Deflector with Reduced Drive Power: Analysis, Design, and Experimental Examination

Yurchenko, A.V.
Oboznenko, V.M.
Moskalev, V.M.

Kiev Taras Shevchenko National University
Radiophysics Faculty
Vladmirskaya St. 64
252033 Kiev, Ukraine

Stevens, D.M.

Avionics Directorate
Electro-Optical Components Branch
Wright-Patterson AFB, OH 45433

SEPTEMBER 1997

FINAL REPORT FOR PERIOD 1/10/96 - 12/9/96

Approved for public release; distribution unlimited

19980410 034

AVIONICS DIRECTORATE
WRIGHT LABORATORY
AIR FORCE MATERIEL COMMAND
WRIGHT-PATTERSON AIR FORCE BASE, OH 45433-7623

DTIC QUALITY INSPECTED 3

NOTICE

USING GOVERNMENT DRAWINGS, SPECIFICATIONS, OR OTHER DATA INCLUDED IN THIS DOCUMENT FOR ANY PURPOSE OTHER THAN GOVERNMENT PROCUREMENT DOES NOT IN ANY WAY OBLIGATE THE US GOVERNMENT. THE FACT THAT THE GOVERNMENT FORMULATED OR SUPPLIED THE DRAWINGS, SPECIFICATIONS, OR OTHER DATA DOES NOT LICENSE THE HOLDER OR ANY OTHER PERSON OR CORPORATION; OR CONVEY ANY RIGHTS OR PERMISSION TO MANUFACTURE, USE, OR SELL ANY PATENTED INVENTION THAT MAY RELATE TO THEM.

THIS REPORT IS RELEASABLE TO THE NATIONAL TECHNICAL INFORMATION SERVICE (NTIS). AT NTIS, IT WILL BE AVAILABLE TO THE GENERAL PUBLIC, INCLUDING FOREIGN NATIONS.

THIS TECHNICAL REPORT HAS BEEN REVIEWED AND IS APPROVED FOR PUBLICATION.

Signature: Dale Stevens 12 MAR 98

Do not return copies of this report unless contractual obligations or notice on a specific document requires its return.

DTIC QUALITY INSPECTED 3

TABLE OF CONTENTS

LIST OF FIGURES

REPORT DOCUMENTATION PAGE

Form Approved
OMB No. 0704-0188

Public reporting burden for this collection of information is estimated to average 1 hour per response, including the time for reviewing instructions, searching existing data sources, gathering and maintaining the data needed, and completing and reviewing the collection of information. Send comments regarding this burden estimate or any other aspect of this collection of information, including suggestions for reducing this burden, to Washington Headquarters Services, Directorate for Information Operations and Reports, 1215 Jefferson Davis Highway, Suite 1204, Arlington, VA 22202-4302, and to the Office of Management and Budget, Paperwork Reduction Project (0704-0188), Washington, DC 20503.

1. AGENCY USE ONLY *(Leave blank)*	2. REPORT DATE	3. REPORT TYPE AND DATES COVERED
	Sep 97	Final 1/10/95 - 8/10/86

4. TITLE AND SUBTITLE
Bragg Cell on TeO(2) for 2-D Deflector with Reduced Drive Power: Analysis, Design, and Experimental Examination

5. FUNDING NUMBERS
C: SPC-95-4036

6. AUTHOR(S)
Yurchenko, A.V., Oboznenko, V.M., Moskalev, V.M.:
Kiev Taras Shevchenko National University
Stevens, D.M.: Avionics Directorate,
Electro-Optical Components Branch

7. PERFORMING ORGANIZATION NAME(S) AND ADDRESS(ES)
Kiev Tara Schevchenko National University
Radiophysics Faculty
Vladmirskaya St. 64
252033 Kiev, Ukraine

8. PERFORMING ORGANIZATION REPORT NUMBER
APC-95-4036

9. SPONSORING/MONITORING AGENCY NAME(S) AND ADDRESS(ES)
European Office of Aerospace
Research and Development
223/231 Old Maryelone Road
London, UK NW1 5th

AVIONICS DIRECTORATE
WRIGHT LABORATORY
AIR FORCE MATERIEL COMMAND
WPAFB, OH 45433-7623
POC: Dale M. Stevens,
AFRL/SNHI, 937-255-7310 x3360

10. SPONSORING/MONITORING AGENCY REPORT NUMBER
WL-TR-97-1192

11. SUPPLEMENTARY NOTES
This is a contract funded by EAORD for the Avionics Directorate, AFMC.

12a. DISTRIBUTION AVAILABILITY STATEMENT
Approved for Public Release; Distributed Unlimited

12b. DISTRIBUTION CODE

13. ABSTRACT *(Maximum 200 words)*
The objective of this work is to study the mechanisms limiting the bandwidth of 2-D Acoustoptic Deflector (AOD) and to examine such a deflector experimentally. The work consists of three parts: 1) The construction of 2-D AOD was considered. The frequency characteristic was analyzed using the physical model of the plane light wave, interacting with the divergent sound beam inside the TeO(2) crystal. The entire frequency characteristic has been calculated, taking into account hte change of the light polarization. The dependence of the frequency characteristic on the acoustic power and constructive parameters of the acousto-optical element have been analyzed. 2) A technique for wide-band matching of the high-frequency LiNbO(3) transducers that allows the exclusion of the impedance transformer has been described and used to match the acousto-optical element on TeO(2). The calculated network was practically constructed and examined experimentally. 3) The 5.5 deg and 7.9 deg acousto-optical deflectors were investigated experimentally. The frequency characteristics at various adjustment angles and drive powers have been measured and analyzed.

14. SUBJECT TERMS
Acousto-optic deflector, TeO(2)

15. NUMBER OF PAGES
36

16. PRICE CODE

17. SECURITY CLASSIFICATION OF REPORT	18. SECURITY CLASSIFICATION OF THIS PAGE	19. SECURITY CLASSIFICATION OF ABSTRACT	20. LIMITATION OF ABSTRACT
UNCLASSIFIED	UNCLASSIFIED	UNCLASSIFIED	SAR

Standard Form 298 (Rev. 2-89) (EG)
Prescribed by ANSI Std. 239.18
Designed using Perform Pro, WHS/DIOR, Oct 94

1.0 Abstract

The frequency characteristic dependence on acoustic power and the constructive parameters of a non-axial Bragg cell have been analyzed using numerical simulations. The numerical results suggest an explanation of the rectangular frequency form, which has been observed by other researchers in experiment when the incident angle is slightly different from the calculated one. Bragg cells with incident angles of 5.5° and 6° were studied. Theoretically, drive power can be reduced by increasing the length of interaction and lowering the operating frequency. 1-D Bragg cell for 2-D construction with crossed cells was fabricated and the theoretical effects were confirmed experimentally. Drive power for the 5.5^0 Bragg cell was half as large as the 7.9^0 Bragg cell; however, its bandwidth was only 27.1 MHz instead of the expected 40 MHz due to a transducer bandwidth limitation.

2.0 Introduction

Acousto-optic (AO) Bragg cells on TeO_2 are widely used in practice. They are especially useful in 2-D deflector with crossed cells because of their fabrication simplicity. But in this case drive power P_{dr} grows significantly because of the decreased L/H ratio (Here L and H are length and height of the acousto-optic interaction ("AOI") domain). It is important therefore to study ways of reducing drive power. There are already a considerable number of papers dealing with the

midband degeneracy (non-axial deflector) was proposed [2], to 1984 there were no attempts to solve any optimization problems for it. Then a set of papers was published [6-9] within which these problems were studied, but the results were only appropriate for deflectors with efficiency less than 0.5. Besides, there were no experimental data in those works. Some experimental results concerning the drive power of the 6° deflector were presented in [2,4,10]; however, there were no grounds in these papers why exactly the 6° interaction was chosen without considering optimization. Recently works appeared [11,12] in which other non-axial deflectors (8°, 9°, 10°) were studied theoretically and experimentally, but they did not specify any data about the drive power.

The objectives of this work are to clarify limiting factors for design of non-axial deflector on TeO_2 with reduced drive power, and experimentally verify the optimum design results in the fabrication of a cell for 2-D deflector with crossed cells.

Our investigations are based on a simple and well known fact that diffraction efficiency improves when either the interaction length L, (or the piezoelectric transducer length) increases (see Fig. 1). Thus, it is possible to decrease P_{dr} increasing L.

Analysis of the deflector frequency characteristic

In order to establish the design limitations for when L is increased, it is necessary to evaluate what happens from this procedure. First, the AOI bandwidth decreases due to reduced sound beam divergence. It is possible to eliminate the effect by lowering an operating frequency, but then we need to take into account other factors which are dependent on frequency in different ways; e.g., polarization of incident light and acoustic loss. In this case acoustic loss only decreases causing increased efficiency, but the incident light ellipticity increases causing reduced efficiency.

Therefore it seems reasonable to lower the operating frequency until the bandwidth stays greater than some given value. We shall analyze the deflector frequency characteristic to clarify

the basic factors that it depends on.

A vector diagram of AOI is shown in Fig. 1. Here curves $|\mathbf{k}_1(\theta)|$ and $|\mathbf{k}_2(\theta)|$ are cross-sections of the light wave vector surfaces by the $(1\bar{1}0)$ plane, θ is an angle between the [001] axis and an arbitrary light vector $\mathbf{k}$. The divergent sound wave is represented by a set of wave vectors $\mathbf{K}(\alpha)$, e.g., $\mathbf{K}_B$, $\mathbf{K}_{N1}$, $\mathbf{K}_C$, $\mathbf{K}_{N2}$, $\mathbf{K}_D$, where α is the angle between the [110] axis and an arbitrary vector $\mathbf{K}$. Efficient AOI occurs when the Bragg conditions are satisfied, i.e., vectors $\mathbf{k}_1(\theta_1)$, $\mathbf{k}_2(\theta_2)$ and $\mathbf{K}(\alpha)$ are closed as it is shown in Fig. 1 for the ABO triangle. The frequency characteristic is formed as a result of the incident light wave vector $\mathbf{k}_1(\theta_1)$ interaction with a set of the sound wave vectors $\mathbf{K}(\alpha)$. Thus, its shape is obviously dependent on the incident angle θ_1, i.e., on the "adjustment angle" of the deflector. (We mean that frequency characteristic can be adjusted by rotation of Bragg cell around the $[1\bar{1}0]$ axis).

Consider Fig. 1 more carefully to analyze this dependence. Varying the angle θ_1 means that the point A travels along the curve $|\mathbf{k}_1(\theta)|$, and the normal to transducer N shifts in parallel to itself. This causes that a length of vector $\mathbf{K}_C$ and an angle α_C between a tangent to the curve $|\mathbf{k}_2(\theta)|$ and the [110] axis are changed, i.e., depend on the angle θ_1. Thus, the frequency $f_C=\mathbf{K}_C(\alpha_C)\cdot v(\alpha_C)/2\pi$ depends on the angle θ_1 in a complicated way (here $v(\alpha_C)$ denotes a sound wave velocity traveling at the angle α_C to the [110] axis). Until now, researchers following Dixon[13] used the condition $\partial\theta_1/\partial f=0$ to find the incident angle θ_1, not taking into account that, in fact, θ_1 is a parameter. For this reason the frequency f_C and the angle α_C had a special significance in the theory of non-axial deflector on TeO_2. They were usually considered as basic parameters when the deflector characteristics were analyzed. Until references 7-9 were published, the usual

way [2-5] was to consider interaction of the plane light wave (vector $\mathbf{k}_1$) with the plane sound wave which was described exactly by vector $\mathbf{K}_C$. It was assumed that $\mathbf{K}_C$ was tangent to the curve $\mathbf{k}_2(\theta)$, and the angle α_C determined all properties of the deflector. It was assumed as well[2] that a bandwidth of AOI is largest in this case. Such an approach by no means took into account divergence of the sound beam. Authors of references 7-9 considering the divergent sound beam and introducing a set of calculated parameters, have proposed the calculation procedure for deflector on TeO_2. They have taken into account a change of the sound divergence when frequency was changed. Using the bounding frequencies f_{min}, f_{max} and efficiency η as initial data, they managed to estimate basic peculiarities of the frequency characteristic and calculate θ_1, α_C, f_C and L. But their approach did not enable one to analyze how the frequency characteristic depended on the angle θ_1, because f_C and α_C depended on the angle θ_1 themselves.

On the other hand, the constructive angle α_N between the normal to transducer N and the [110] axis is determined only by the Bragg cell construction and can not be varied after deflector fabrication (on the contrary, the angle θ_1 may be adjusted). Until now the angle α_N was considered to be completely identical to the angle α_C, e.g., it was assumed to be equal to 6° [2,4,5,10]. Of course, that was only valid in the special case when the normal N was tangent to the curve $|\mathbf{k}_2(\theta)|$, and the angle θ_1 was rigorously equal to a certain value. Thus, it is impossible to analyze the dependence of frequency characteristic on the angle θ_1. The decision is to consider the angles α_N and θ_1 as basic parameters and analyze the frequency characteristic varying them. Using the constructive parameter α_N instead α_C makes this possible. This approach enables one to distinguish the influence of different parameters on a frequency characteristic shape.

In real construction, the angle θ_1 is not changed after adjusting the deflector. But it is obvious

that if the angle θ_1 is fixed (i.e., the point A is tied to its place), the length of an arbitrary vector**K** and its direction will be correlated unambiguously. In other words, the angle α, determining directions of vectors **K**, for which Bragg conditions are performed, will depend on frequency, i.e. $\alpha=\alpha(f)$ when θ_1 is a parameter.

The dependence of Bragg angle Θ (see, e.g., the angle Θ_N for the wave vectors $\mathbf{K}_{N1,2}$ in Fig. 1) vs frequency is determined by Dixon's equations (in form [4]):

$$\Theta(f,\alpha(f,\theta_1)) = \frac{\lambda \cdot f}{2 \cdot n_1(\theta_1) \cdot v(\alpha(f,\theta_1))}[1 + v^2(\alpha(f,\theta_1)) \frac{n_1^2(\theta_1) - n_2^2(\theta_2(f,\alpha(f,\theta_1))}{(\lambda \cdot f)^2}], \quad (1)$$

$$\text{where} \quad \theta_2(f,\alpha(f,\theta_1)) = \theta_1 + \frac{\lambda \cdot f}{n_o \cdot v(\alpha(f,\theta_1))} . \quad (2)$$

(We have written $v = v(\alpha)$ in these equations to emphasize the strong dependence of the sound velocity on the direction of **K** near the [110] axis in TeO_2.) Here λ is the light wavelength in vacuum, $n_1(\theta_1)$ and $n_2(\theta_2)$ are indexes of refraction for incident and diffracted light beams accordingly, n_o is an index of refraction for an ordinary beam. Substituting (2) into (1) and taking into account that $\alpha = \Theta + \theta_1$ yields, after the performing the required algebra, a functional equation with regard to $\alpha(f,\theta_1)$:

$$\alpha(f,\theta_1) - \theta_2(f,\alpha(f)) = \Theta(f,\alpha(f,\theta_1)) - \frac{\lambda \cdot f}{n_o \cdot v(\alpha(f,\theta_1))} . \quad (3)$$

Now one can find $\alpha(f,\theta_1)$ solving equation (3) and then calculate frequency characteristic, but it seems to be rather complicated. We use another procedure instead considering coupled numerical arrays α_j, f_j and constructing numerical function $\alpha(f)$ with θ_1 as a parameter. This procedure is described completely in the appendix.

If the transmission losses *TL* of electro-acoustic transducer are not dependent on frequency, the acoustic power P_a of the plane sound wave interacting with the plane incident light wave will

only depend on the difference $\Delta\alpha = \alpha - \alpha_N$. The efficiency of the acousto-optical interaction in that case

$$\eta_0(f,\Delta\alpha) = \sin^2[\frac{\pi L}{\lambda\cos(\Theta(f))}\sqrt{\frac{M_2 P_a}{2LH}}\cdot F(f,\Delta\alpha)] , \tag{4}$$

where $\Theta(f) = \alpha(f) - \theta_1$, and

$$F(f,\Delta\alpha) = \frac{\sin(\pi X(f,\Delta\alpha))}{\pi X(f,\Delta\alpha)} , \qquad X(f,\Delta\alpha) = \frac{L\cdot\Delta\alpha\cdot f}{v} , \tag{5}$$

are functions reflecting an influence of the transducer pattern in the plane of interaction, and M_2 is a figure of merit. But the dependence $\alpha(f)$ is already calculated, and replacing $\Delta\alpha$ into $\Delta\alpha(f)$ and v into $v(\alpha(f))$ in (4), & (5) yields the frequency characteristic $\eta_0(f)$ describing efficiency of AOI inside the crystal. To take into account the reduction of efficiency because of changing the polarization state, it is enough to use equations [14]

$$I_r(\theta) = \frac{1}{1+\xi^2(\theta)}\cdot I_0 , \qquad \xi(\theta) = \frac{\Delta n_a(\theta)}{\Delta n_b(\theta) + \sqrt{\Delta n_b^2(\theta) + \Delta n_a^2(\theta)}} ,$$

$$\Delta n_a(\theta) = (n_1(0) - n_2(0))\cdot\cos^2\theta , \qquad \Delta n_b(\theta) = (n_e(0) - n_o(0))\cdot\sin^2\theta \tag{6}$$

where I_0 is the intensity of the input linearly polarized light, i.e., the incident light out the crystal, $\xi(\theta)$ is ellipticity of the elliptically polarized light with intensity $I_r(\theta)$ in TeO_2. Thus the "ultimate" frequency characteristic depending on parameters α_N and θ_1 is

$$\eta(f,\alpha_N,\theta_1,P_a) = \eta_0(f,\alpha_N,\theta_1,P_a)\cdot I_r(\theta_1)/I_0 . \tag{7}$$

Now, one can analyze it using acoustic power P_a, constructive parameters α_N, L, H and the adjustment parameter θ_1 as initial data. The entire frequency characteristic will be obtained as a result.

Such an analysis has been completed for deflectors at λ=633 nm and 514 nm. The results are presented below, (note here that there was no need to take into account a midband degeneracy in the frequency range considered [9]).

We used the TeO_2 material constants in calculations as follows[1, 4, 14, 15]. Density, kg/m^3, ρ = 5990; Elastic stiffness constants, Newton/m^2, $c_{11} = 5.57 \cdot 10^{10}$, $c_{12} = 5.12 \cdot 10^{10}$, $c_{44} = 2.65 \cdot 10^{10}$; Specific optical rotation, deg/m, $R = 87 \cdot 10^3$ (λ = 633 nm), and $R = 157 \cdot 10^3$ (514 nm); Indexes of refraction $n_o = 2.2597$ (633 nm), $n_o = 2.312$ (514 nm), $n_e = 2.4119$ (633 nm) $n_e = 2.474$ (514 nm);

The figure of merit for the linearly polarized light was assumed to be equal to $M_2 = 700 \cdot 10^{-15}$ sec^3/kg. Its measured value near the [001] is equal to 800-1000 [14], but we used a lesser value to provide some reserve in the calculated efficiency when θ_1 does not vanish, (of course M_2 would have been calculated exactly for the certain θ_1 value if all components of the photoelastic tensor had been known exactly, but different sources give differences up to 50%).

Fig. 2 represents the general shape of the frequency characteristic calculated within the range 30-140 MHz when the transducer pattern orientation is similar to that shown in Fig. 1. There are three curves: 1 - the "ultimate" frequency characteristic $\eta(f)$. It takes into account the reduction of efficiency due to the changing of incident light polarization [14] when it is propagating at an angle θ_1 from the [001] axis; 2 - frequency characteristic without that effect $\eta_0(f)$. Comparing curves 1 and 2 one can see the reduction of efficiency caused by the effect mentioned above; 3 - the frequency characteristic under very small efficiency $F(f)$ normalized to unity.

In fact, curve 3 is an image of the transducer "dynamic" far-field pattern. The pattern is changed itself when frequency is changed. There is no interaction when the angle $\alpha(f) < \alpha_C$, and efficiency is determined by a difference $\Delta\alpha = \alpha - \alpha_N$. If the transducer pattern is located as it is shown in Fig. 1, the maximal efficiency η_{max} is obtained at two frequencies f_{peak1} and f_{peak2} (vectors $\mathbf{K}_{N1}$ and $\mathbf{K}_{N2}$). The dip (note, it is not because of midband degeneracy[1]) at frequency $f=f_M$ disappears when $\alpha_N=\alpha_C$, but only half of the pattern "works" then causing reduction of bandwidth.

The frequency characteristic in this case always images only a part of a pattern, which is located below vector $\mathbf{K}_C$, but twice. For the first time it occurs in the low-frequency range, and for the second time in the high one. So the frequency characteristic would have appeared exactly as two mirror images relative to the vertical line traveling through the frequency f_C if the transducer pattern shape had not depended on frequency, (note here that our analysis does not take into account acoustic loss).

Figure 2 represents the optimum frequency characteristics in such a sense that a bandwidth $\Delta f=f_{max}-f_{min}$ has a maximum value for a certain value of $\eta_M=\eta(f_M)$. It was obtained by varying the θ_1 parameter for the deflector with L=3 mm, H=3 mm, α_N=6°, P_a=200 mW. This is exactly one described in reference [2] but a more precise angle θ_1=4.375° provides a maximal bandwidth Δf=48.3 MHz with η_M=0.803 (see curve 1). The side peaks (above 100 MHz and below 30 MHz) describe AOI with side lobes of the transducer pattern. One also observes a few percent decrease in efficiency because of the incident light ellipticity (compare curves 2 and 1).

Now one can analyze how the frequency characteristic is changed when the constructive parameters and acoustic power are varied, assuming that the Bragg cell is to be used in a 2-D deflector with crossed cells. Then $H=D$, where D is an input light beam diameter, and resolution (by Rayleigh) $N=H\Delta f/v(\alpha_N)$. Further, a Bragg cell will be considered with the resolvable spot number N>512. The characteristics of such a 6° deflector is presented in Fig. 3 (a). Naturally it was necessary to increase P_a up to 450 mW in the calculation to save the efficiency, because L/H is only equal to 0.5 in this case. The P_a value and θ_1=4.353° gives the maximum bandwidth Δf=59.6 MHz with the minimum efficiency, which was assumed to be η_M>0.707, to obtain a common efficiency of more than 0.5 for a 2-D deflector

Figure 3 (b) represents how the frequency characteristic is varied when P_a increases. The central dip goes up and almost disappears, but two other lateral dips appear in the sides (curve 1, P_a=800 mW). This happens because of the nonlinear dependence of $\eta(P_a)$. The central dip disappears completely, when P_a goes up, but the lateral dips go down (curve 2, P_a=1100 mW). They are located exactly at the frequencies f_{peak1} and f_{peak2}, i.e., at the frequencies of the maximum P_a in the transducer pattern (curve 3). Thus, when P_a goes up to some value of P_{amax} on the normal to the transducer, the efficiency η goes over a maximum and then decreases. At the same time, the efficiency of the light interaction with the less power sound wave in the center of the frequency characteristic still only gets its maximum value. This effect is practically useful to get a uniform frequency characteristic, but requires an increased P_a to use it.

Now consider what happens if the θ_I value is slightly different from appointed, i.e. the deflector adjustment is not performed precisely. (Note here that the θ_I angle was calculated with precision to thousands of degree.) In Fig. 4 two such cases are shown. It is seen that very small changes in θ_I (a few hundredth of degree) cause considerable changes in $\eta(f)$. The case when the transducer pattern is "looked through" by the light beam almost completely twice is presented by curve 1. It is observed in the experiment as a bifurcation of a light line produced by the scanning beam on the screen. Such an adjustment means that the normal to transducer N is located far from a tangent to the curve $|\mathbf{k}_2(\theta)|$. The second case (curve 2) gives a short bright line. This is just a case, described above, when half of a transducer pattern works and the normal N is located on a tangent, i.e., the case which was usually analyzed [2-5,11] as to be necessary to obtain maximum bandwidth. One can see however, that that is not optimal for this purpose. From the analysis done above, it becomes obvious as well the cause for getting the rectangular frequency characteristic shape observed by many authors [2,4,10,11] when the incident angle θ_I is slightly

different from calculated one. Actually, their approach used for θ_1 calculation is just the last analyzed case. Thus by slightly decreasing θ_1, they obtained the result described.

Optimal deflector design

One can not make an effective design without first being aware of the basic constructive parameters affecting deflector performance and understanding their effects. So we need to formulate some criteria of optimal design and define corresponding procedures. (Note here that optimal design means to chose constructive parameters of Bragg cell and "to put" the main lobe of a transducer pattern onto curves $|\mathbf{k}_2(\theta)|$ and $|\mathbf{k}_1(\theta)|$ in the best way). From an analysis made above, it follows that such criteria can not be universal ones and an attempt to minimize P_{dr} without taking into account the other deflector parameters seems to be unreasonable. Yet it can be made, if one assumes only a few basic parameters. They may be η_M, N, and Δf.

Assume for example, $\eta_M > 0.707$, $N > 512$, $\Delta f > 40$ MHz. Now varying L, H, α_N, P_a and making a precision adjustment of θ_1 to get the required parameters, a suitable deflector construction can be found. The acoustic power can be considered in that case as a result.

Results of such a procedure for 6° and 5.5° deflectors are represented in Fig. 5 and 6. Here (in figures) $f_{tr} = \sqrt{f_{min} \cdot f_{max}}$ is an operating frequency of the electro-acoustic transducer and $\Delta f_{tr} = (f_{max}-f_{min})/f_{tr}$ is its required relative bandwidth.

Consider the obtained data more carefully. Inspection of the calculation results for different constructive versions of deflectors with the same angle α_N and similar performances (Fig. 5, curve 1 and 2) indicates that generally speaking, θ_1 and f_{tr} depend on L, but the last dependence is not strong. However, the relative bandwidth of the transducer is essentially greater in case 1, when L is less. On the other hand, its surface $S=L\times H$ is almost half the size in that case; therefore, from

the point of view of the electro-acoustic efficiency, it can not be said unambiguously which case is better. The ultimate conclusion can be made only after experimental examining of a designed deflector.

The frequency characteristic of the 6° deflector with a usual transducer (curve 1 in Fig. 5, L = 3 mm) indicates as well that apparently P_a may be reduced by loosing in bandwidth Δf, which is much greater than 40 MHz.

It is also seen that the 6° deflector with L = 5 mm (curve 2) is an almost optimum one in the mentioned sense, but there is still some reserve in the bandwidth which can be used to reduce P_{dr} further. Results of such an attempt are represented in Fig. 6 (curve 1). The given requirements are practically completely obtained by construction of the 5.5°. Actually, acoustic power P_a = 320 mW is the lowest, and other parameters are suitable too. Besides, further reduction of P_a is not merely possible because of unacceptable deterioration of other parameters.

Fig. 6 (curve 2) also shows an efficiency characteristic of the 5.5° deflector at λ = 514 nm, designed from the same criteria. It is located in a much higher frequency range. It means that the same optimal deflector can not be used for the different wavelengths provided the super-wide-band transducer is used. But, in this case the transducer efficiency certainly has to be less.

Note that in fact, an iterative process has been used to obtain the required frequency characteristic at λ=633 nm. At first, some angle α_N<6° and length of interaction were chosen, then the frequency characteristic and its bandwidth Δf were calculated The angle θ_1 was varied at some reasonable P_a value, and at last the height of interaction H to obtain N>512 at the Δf was chosen. Finally, θ_1 and P_a values were found precisely. Probably the same process for λ=514 nm could lead to a better result with another α_N, e.g. in case of α_N=5° or 6°.

Experimental investigations of the 5.5° deflector

The frequency characteristics $\eta(f)$ at different drive power levels were measured using the experimental setup shown in Fig. 7. It consisted of the connected electrical and optical parts. The electrical part included the deflector driver, the universal I/O interface, the radio-frequency counter, and the power meter. The driver and the I/O interface have been located inside the PC. The power meter and the counter were standard instruments that were connected to the computer through the I/O interface.

The deflector drive power was measured indirectly. We imply here the drive power as an available power of the drive signal source, i.e., the power that the generator can give out into the matched load. In that case P_{dr} can be measured independently, and different deflectors can be compared working with different drivers. Thus, the P_{dr} value was determined as an output power of a signal source (a driver or a generator), which drove a deflector to provide special characteristics.

The driver had output power up to 900 mW within the frequency range 40 - 90 MHz . Its output impedance was not measured; therefore, it was necessary to use the external attenuator. The 3 or 6 dB value attenuators have been used. The uniformity of the output $P_{dr}(f)$ characteristic within the ± 0.5 dB was provided with the special calibrating procedure. It consisted in the measuring of the output power at the 32 fixed frequencies and controlling by power until its given value had been achieved. While this procedure was carried out, the driver output was connected to the power meter, not to the deflector.

The power meter input impedance was equal to 50 ohm as were all the cables used. Thus, the P_{dr} value measurements with the 50 ohm feeder have been performed. The precision of the power meter itself was within ± 8 %.

The optical part was mounted on an optical bench. The linearly polarized He-Ne laser was setup in a way to allow rotation around its axis, changing the electrical vector **E** orientation in the incident light beam.

An experimental sample at λ=633 nm was fabricated from a single crystal of TeO_2 with common sizes 26×25×13 mm^3 and the constructive parameters are given in Fig. 8. Its optical surfaces were covered by SiO_2 antireflection coating. In this construction, the incident outside angle i is equal to the constructive angle β, which can be calculated from the obvious equation

$$\arcsin[n_1(\theta_1)\cdot\sin(\beta+\theta_1-\alpha_N)]-\beta=0 \qquad (8)$$

to provide an output angle $\theta_{out}(f)$= $\arcsin[n_2(\theta_2(f))\cdot\sin(\theta_2(f)-\alpha_N)]$ equal to 0 at some central frequency within operating range when $\theta_2=\alpha_N$. The constructive angles were fabricated within ±5 angle second. The shear-wave transducer was fabricated from the 163° $LiNbO_3$ plate that was bonded to the TeO_2 element by means of the vacuum diffusion welding, and then was ground up to the required thickness.

According to the results obtained in the numerical simulation above, the examined deflector had the angle α_N equal to 5.5°. Its transducer with operating frequency f_{tr}=55.8 MHz had a surface S=6(L)×8 mm^2 and had been matched by means of the third order transformerless optimal matching network[16]. Measured and calculated dependencies of voltage standing wave ratio ("*VSWR*") vs frequency are represented in Fig. 9. Curve 1 is the calculated *VSWR* of the matched transducer, but not the *VSWR* of the equivalent circuit. It has been calculated as an input *VSWR* of the matching network loaded by the transducer input impedance found experimentally. The difference between input impedances of the transducer and its equivalent circuit causes the distortion of the frequency characteristic compared with the ideal Tchebysheff one. The calculated

matched bandwidth Δf_{mtch} = 29.4 MHz (40.4-69.8 MHz, $VSWR_{max}$ =2.41) has been obtained with this transducer instead of the expected 40 MHz value. Curve 2 is the measured *VSWR* of the real matching network constructed as a lumped one. The maximal *VSWR* level within the matched bandwidth Δf_{mtch} = 32.3 MHz (39.8 - 72.1 MHz) was equal to 2.51.

We note here that the measured quality factor Q=5.21 appeared to be unexpectedly large. Thus, this large value of Q together with rather low operating frequency f_{tr}=55.8 MHz were the reasons prevented attainment of the expected bandwidth.

The Bragg cell was mounted so as to provide a precise rotation around two perpendicular axes. The precision adjustment around the main axis allowing adjustment of the angle $\theta_{adj} \approx \theta_1 \cdot n_1(\theta_1)$ was within ± 9 angle seconds. The laser beam was expanded by the telescope and then was limited by an aperture (diaphragm) 8 mm in diameter. The linearity of the photodiode was provided by the red optical filter with the necessary attenuation located before it. The measured frequency characteristic $\eta(f)$ was imaged on the computer display and was recorded into the disk. Typical displayed images are represented below.

As was mentioned above, there is a maximum acoustic power level that when exceeded gives an efficiency decrease. The corresponding drive power P_{drmax} level was found to be about 410 mW. Therefore the $\eta(f)$ characteristics at various θ_{adj} have been measured while the calibrated P_{dr} was equal to 400 mW. They are presented in Fig. 10. The best characteristic (curve 2) obtained with some angle $\theta_{adj}=\theta_{adj0}$ provided a deflector bandwidth of Δf=27.1 MHz (44.2 - 71.3 MHz) at the level η_M=0.45 with maximum efficiency η_{max} = 0.68. The high bounding frequency f_{max}=71.3 MHz was determined by the transducer band, but the low bounding frequency f_{min}= 44.2 MHz was apparently limited by the transducer pattern width. Note that there is a peak efficiency at the frequency of f_{peak1}=49.6 MHz described above (see Fig. 2 as well), but it is absent in the high-

frequency part of the characteristic curve. Two other device characteristics were obtained for θ_{adj} varying by $\pm 3'$. Curve 1 represents the case when the pattern of the transducer is "looked through" twice by the light wave. The low-frequency peak is well observed, but the high-frequency one is absent because of the limited transducer bandwidth. Curve 3 represents the case when only half of the transducer pattern works. Differences between the calculated and measured characteristics are discussed below.

Figure 11 shows the behavior of the $\eta(f)$ characteristic when the drive power is changed. The P_{dr} values were 200, 400, 600 mW and the adjustment angle θ_{adj} was equal to θ_{adj0}. As mentioned, the output power of the driver was limited by the value 900 mW; therefore, the external attenuator can not be used in the last case. Owing to this reason, the efficiency characteristic obtained at 600 mW has an illustrative significance. The effect of the deterioration of the essential efficiency characteristic when $P_{dr} > P_{drmax}$ is clearly observed. It occurs already at the P_{dr} =600 mW (curve 3). It is also seen that the P_{dr} value equal to 400 mW is close to the best one for the examined deflector. Actually, an increase in drive power up to 600 mW does not cause an increased η_{max}, and the bandwidth Δf increases only from 27.1 to 29.4 MHz in that case.

Measurements of 7.9° Bragg cell characteristics with an operating frequency f_{tr} =85 MHz have been performed (see Fig.12) to compare drive power reduction in the 5.5° device in spite of the limited driver maximum frequency of 90 MHz. In this case, even P_{dr} =800 mW was less than $P_{drmax} \approx$ 980 mW at f=73 MHz, which was measured using an additional generator. Note as well that the η_{max} value of the 7.9° deflector was less than the η_{max} value of the 5.5° deflector (0.60 and 0.68 correspondingly).

Discussion of Results

In spite of a good qualitative agreement between measured and calculated frequency characteristics, quantitatively they are strongly different. First of all, the experimentally obtained efficiency is much less than the calculated one. Moreover, we could not obtain improved efficiency by increasing the drive power. Apparently it can be caused by an acoustic loss which has not been taken into account in the model used. Actually, in the case of an arbitrary acoustic power the normalized efficiency of light diffracted under Bragg angle [17]

$$\zeta = \frac{1}{D}\int_0^D \sin^2\left[\frac{\pi \cdot P}{2}\exp(-\alpha z)\right]dz \ , \tag{9}$$

where $$P = qL/\pi \ , \quad q = \frac{\pi}{\lambda \cdot \cos\Theta}\sqrt{\frac{M_2 \cdot P_a}{L \cdot H}} \ , \tag{10}$$

α is the acoustic loss factor. Assuming that α is directly proportional to f-square and using the acoustic loss value equal to 16 $dB \cdot sec^{-1} \cdot MHz^{-2}$ [1] for shear waves along the [110] axis, one can calculate the frequency dependence $\zeta(f)$ at various levels of P_a. Note that the ζ value depends on the constructive parameter H, not only because of (9), but also it follows from $H = D$ in the 2-D construction as far as common acoustic loss on the aperture depends on H. Taking into account this fact, it is interesting to compare the examined deflector with the best one described in reference 2. It is the 6° deflector with the transducer 3 by 3 mm. Its efficiency was equal to 0.80 at the P_{dr} = 350 mW. Using it in a 2-D construction one can obtain the resolution N=223, because of the small H value. The 5.5° cell provides N=337 even at the obtained Δf = 27.1 MHz, but its maximum efficiency is equal only to 0.68. Thus, it is necessary to perform additional investigations to find the actual optimum construction.

Curves calculated using (9) are represented in Fig. 13. Curve 1 describes the 6° deflector[2]. One can see a good agreement with this curve and experimental results[2]. The P_a value equal to 320 mW for the 5.5° device (curve 2) was chosen from the calculation done above (see Fig. 6). The L and H values were chosen in a similar manner. Significant efficiency reduction is observed as well. Note that the higher efficiency of the 6° deflector compared with the 5.5° deflector is observed because of the higher H value in the second case (8 mm against 3 mm). Thus, less efficiency is a payment for saving the given N>512 value in 2-D construction. The P_a value equal to 700 mW (curve 3) for the 7.9° Bragg cell was used assuming that the best P_{dr} value is about 900 - 950 mW and the transmission loss of the transducer is approximately equal to the transducer loss of the 5.5° deflector.

Experiment confirmed the strong dependence of the $\eta(f)$ characteristic on the angle θ_{adj} as well. At the same time, the essential difference in the entire characteristic shape is observed for calculated and measured curves, and if the lack of a high frequency peak on curve 1 can be explained from the limited transducer bandwidth, the behavior of the measured characteristics in the domain A (see Fig. 10) has no reasonable explanation. Actually, the peak on curve 2 is not observed and there is even a slope in this place on curve 3. The efficiency reduction in the last case compared with curves 1 and 2 is also not explained. Perhaps some of these differences are caused by the transducer pattern distortion because of non-uniform sound field distribution.

Conclusions

From the obtained results one can make following conclusions.

(1) In TeO_2, parameters of the usually used physical model α_C, f_C depend only on the parameter θ_1 (the angle between [001] and the incident light wave vector) if the AO interaction occurs in the

$(1\bar{1}0)$ plane. (2) Using an additional constructive parameter α_N (the angle between [001] and the normal to transducer) in this model, one can analyze the efficiency frequency dependence $\eta(f)$ on the different factors separately. It is impossible if only the usual parameters of the physical model α_C and f_C are used. (3) One ought not use bounding frequencies as initial data if an optimal design is to be made. Only the bandwidth of the deflector has to be given. (4) The true optimal design may be made only for a given light wavelength. The same Bragg cell can not be optimal for different λ. (5) The physical model used correctly describes the main peculiarities of the frequency characteristic, but some effects observed experimentally can not be explained in its frame. There is no reasonable explanation for the characteristic distortion in the high-frequency domain. (6) The design approach used allows one to obtain the optimum essential reduction of the drive power. At least P_{dr}=400 mW per channel can be achieved for 2-D Bragg cell construction with a bandwidth of about 30 MHz and resolution more than 512 at λ=633 nm. The 5.5° deflector is suitable for this purpose.

Appendix. Calculation of Bragg cell frequency characteristic

The dependence of the sound velocity v on the angle α between the arbitrary sound wave vector **K** and the [110] axis (Fig. A1) is described by[9]

$$v(\alpha) = \sqrt{\frac{1}{\rho}\cdot\left(\frac{c_{11}-c_{12}}{2}\cdot\cos^2\alpha + c_{44}\cdot\sin^2\alpha\right)}\ . \qquad \text{(A1)}$$

In turn, the dependence of the indexes of refraction n_1 (slow wave) and n_2 (fast wave) on the angle θ between the light wave vector **k** and the [001] axis are [9]

$$n_1(\theta) = n_{01}(\theta) + \frac{1}{2}\cdot n_{01}^3(\theta)\cdot\rho(\theta)\cdot G(\theta)\ , \qquad n_2(\theta) = n_{02}(\theta) - \frac{1}{2}\cdot n_{02}^3(\theta)\cdot\rho(\theta)\cdot G(\theta)\ . \qquad \text{(A2)}$$

Here $G(\theta) = \dfrac{R \cdot \lambda \cdot \cos^2\theta}{\pi \cdot n_o^3}$, $n_{01}(\theta) = \dfrac{n_e \cdot n_o}{\sqrt{n_e^2 \cdot \cos^2\theta + n_o^2 \cdot \sin^2\theta}}$, $n_{02}(\theta) = n_o$,

$$\rho(\theta) = \frac{\sqrt{\left(n_o^{-2} - n_{01}^{-2}(\theta)\right)^2 + (2 \cdot G(\theta))^2} - (n_o^{-2} - n_{01}^{-2}(\theta))}{2 \cdot G(\theta)} .$$

The lengths of the sound wave vectors are equal to the lengths of segments AB, AC and AD in Fig. A1. The equations for lines $P(\theta)$ (the tangent) and $P_{sec}(\theta)$ (the secant) in polar coordinates can be easily written from the triangles ACO, APO and AC′O, AP′O as the lengths of the segments OP and OP′

$$P(\theta, \alpha_C) = n_2(\alpha_C) \cdot \cos^{-1}(\alpha_C - \theta) , \tag{A3}$$

$$P_{sec}(\theta, \alpha) = n_1(\theta_1) \cdot \cos(\alpha - \theta_1) \cdot \cos^{-1}(\alpha - \theta) . \tag{A4}$$

As it is seen from Fig. A1, the location of the point A on the curve $n_1(\theta)$ unambiguously determines the location of the tangent $P(\theta)$ and the couple of values α_C and θ_1. The condition OA=OP at $\theta=\theta_1$ and equation (A3) immediately yields an equation to establish a connection between α_C and θ_1

$$n_1(\theta_1) - P(\theta_1, \alpha_C) = 0 . \tag{A5}$$

Given the array of the α_{Cj} values, the array of the θ_{1j} values can be found as solutions of equation (A3). Then the lengths of segments $AC_j = |\mathbf{K}(\alpha_{Cj})|$ can be calculated from the triangle ACO, and the array of the f_{Cj} values from the known $\mathbf{K}(\alpha_{Cj})$ and the equation

$$f_{Cj} = v(\alpha_{Cj}) \cdot \lambda^{-1} \cdot n_2(\alpha_{Cj}) \cdot \tan(\alpha_{Cj} - \theta_{1j}) . \tag{A6}$$

Now having coupled arrays α_{Cj}, θ_{1j}, and α_{Cj}, f_{Cj}, there is a possibility to calculate numerical functions $\alpha_C(\theta_1)$ and $f_C(\theta_1)$ using interpolation by cubic splines. This procedure has been made by means of the MATHCAD 5.0 PLUS[18] application.

The numerical functions $\alpha(f)$ and $\theta_2(f)$ can be calculated in the same way using the equation

$$n_2(\theta_B) - P_{sec}(\theta_B, \alpha) = 0 \tag{A7}$$

to find the array of θ_{Bj} values. The array of f_{lowj} values was found from the triangle AEO:

$$f_{lowj} = v(\alpha_j) \cdot \lambda^{-1} \cdot \sqrt{n_1^2(\theta_1) + n_2^2(\theta_{Bj}) - 2 \cdot n_1(\theta_1) \cdot n_2(\theta_{Bj}) \cdot \cos(\theta_{Bj} - \theta_1)} \ . \tag{A8}$$

Here f_{low} denotes the low-frequency range $f \leq f_C$. The frequencies f_{high} from the high-frequency range $f > f_C$ were calculated by replacing θ_B into θ_D in equations (A7), (A8) and making the same calculations. The coupling of the α_j, f_{lowj}, and α_j, f_{highj} arrays yielded numerical functions $\alpha(f_{low})$ and $\alpha(f_{high})$ which then have been unified into one function $\alpha(f)$. The same procedure for the α_j, θ_{Bj}, α_j, θ_{Dj} and α_j, θ_{Ej} arrays have yielded numerical functions $\theta_2(f)$, $\theta_E(f)$.

Thus the numerical functions $\alpha(f)$, $\theta_2(f)$ and $\theta_E(f)$, with parameter θ_1, were obtained as a result. This makes it possible to calculate the entire frequency characteristic $\eta(f)$, the degeneracy frequency f_{dgnr} and the output angles of Bragg cell $\theta_{out}(f)$.

This research was sponsored by the US European Office of Aerospace Research and Development, special contract SPC-95-4036. The authors gratefully acknowledge V.A. Goncharov, L.N. Ilchenko and E.N. Smirnov for development and adjustment of measurement equipment.

References

1. Warner A.W., White D.L., Bonner W.A. Acoustooptic light deflectors using optical activity in paratellurite // J. Appl. Phys., vol. 43, no. 11, p.4489-95 (1972)

2. Yano T., Kawabuchi M., Fukumoto A., Watanabe A. TeO_2 acoustooptic Bragg light deflector without midband degeneracy // Appl. Phys. Lett. (USA), vol.26, no.12, p.689-91 (1975)

3. Bryjina M.F., Yesayan S.Kh. Anisotropic acoustooptic deflector on one-axis crystal with optic activity // Zh. Tekh. Fiz. (Russia), vol.47, no.9, p.1937-43 (1977)

4. Tischenko Yu.N., Trubetskoy A.V. Problems of creation and investigation of acoustooptic deflector on TeO_2 single crystals // Avtometriya (Russia), no.1, p.87-95, (1979)

5. Semenkov V.P. Anisotropic acoustooptic deflector on one-axis crystal with optic activity // Zh. Tekh. Fiz. (Russia), vol.51, no.10, p.2090-95 (1981)

6. Bogdanov S.V. Optimization of light acoustooptic deflectors //Kvantovaya elektronika (Russia), vol.11, no.7, p.1481-83 (1984)

7. Bogdanov S.V., Bolsheva T.A. Calculation of basic parameters of acoustooptic deflector on TeO_2 // Avtometriya (Russia), no.5, p.34-41, (1985)

8. Bogdanov S.V. Conditions for arising of the repetitive diffraction and its influence on the work band of acoustooptic deflector//Avtometriya (Russia), no.5, p.41-49, (1985)

9. Bogdanov C.V. Technique to calculate an acoustooptic deflector on paratellurite // In the book: Acoustooptic devices of radioelectronic systems.- Leningrad (Russia): Naul'a (Science), 1988.- p. 61-71

10. Vanushev B.V., Tarkov V.A., Shipov P.M. Acoustooptic deflector // Avtometriya (Russia), no.5, p.29-34, (1985)

11. Eloev E.N., Zubov V.A., Tavasiev A.F., Torgashin A.N., Chalikidi N.K. Investigation of efficiency of acoustooptic paratellurite deflectors //J. Sov. Laser Res. (USA), vol.13, no.6, p.463-71 (Nov.-Dec. 1992)

12. Bikovskiy Yu.A., Eloev E.N., Kukharenko K.L., Panin A.M., Solodovnikov N.P., Torgashin A.N., Arestova E.L. Specialized acousto-optical processor for input, display and coherent-optical processing of multiparameter information from spaceborn telemetric systems // Kvantovaya elektronika (Russia), vol.22, no.10, p.964-70 (1995)

13. Dixon R.W. Acoustic diffraction of light in anisotropic media. // IEEE J. Quant. Electr., vol. QE-3, p. 85-93 (1967)

14. Yano T., Watanabe A. Acousto-optic figerfigure of merit of TeO_2 for circularly polarized light // J. Appl. Phys. (USA), vol. 45, no. 3, p. 1243-45 (1974)

15. Acoustic crystals. Handbook. - Ed. Shaskol'skaya M.P. - Moscow (Russia): Nauka (Science), 1982. - P. 632

16. Yurchenko A.V. Wide-band transformerless matching of high-frequency piezotransducers // Izv. Vyssh. Uchebn. Zaved. Radioelektron. (Ukraine), no.7, p. 41-48 (1995)

17. Balakshiy V.I., Parygin V.N., Chirkov L.E. Physical foundation of acoustooptics.- Moscow (Russia): Radio i svyaz (Radio and communication), 1985, p.139

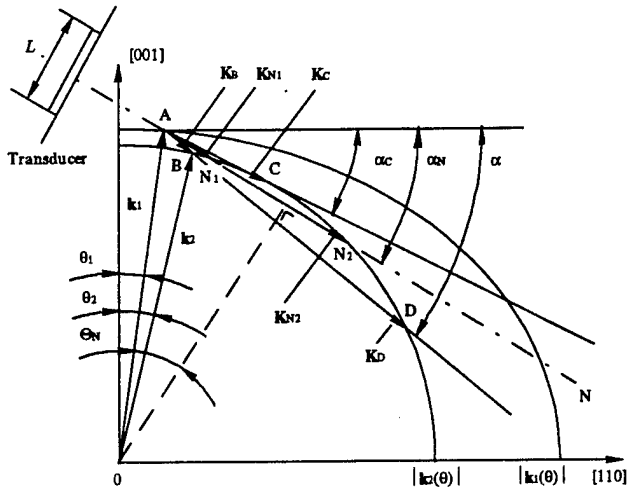

Fig. 1. The vector diagram illustrating acousto-optical interaction of the plane light wave with divergent sound beam in TeO_2. $\mathbf{k}_1$ - wave vector of incident light; $\mathbf{k}_2$ - wave vector of deflected light; $\mathbf{K}$ - wave vectors of sound; N - normal to the transducer; Θ_N - Bragg angle for the sound vectors lying on the normal N.

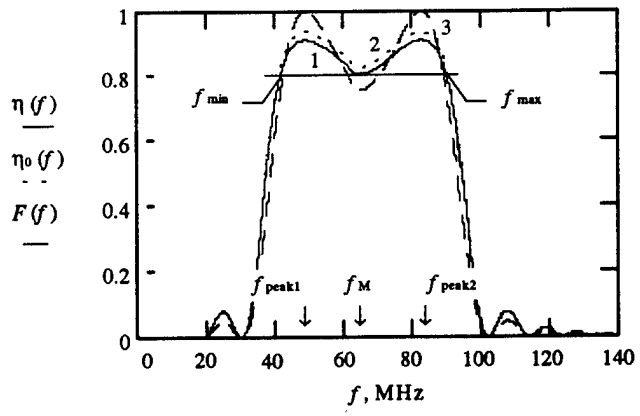

Fig. 2. Typical frequency characteristic of TeO_2 deflector. L=3 mm, H=3 mm, α_N=6°, θ_1=4.375°; P_a=200 mW.

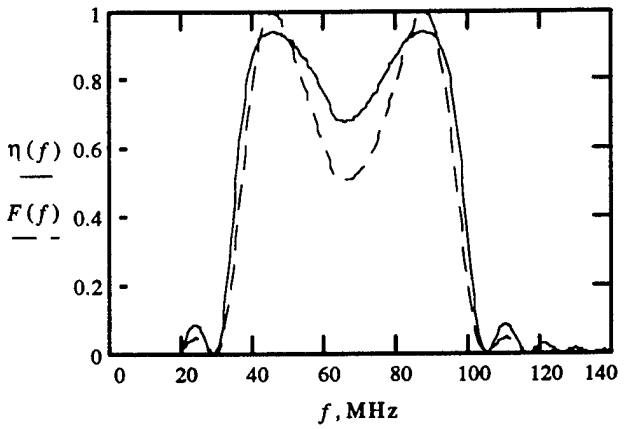

(a)

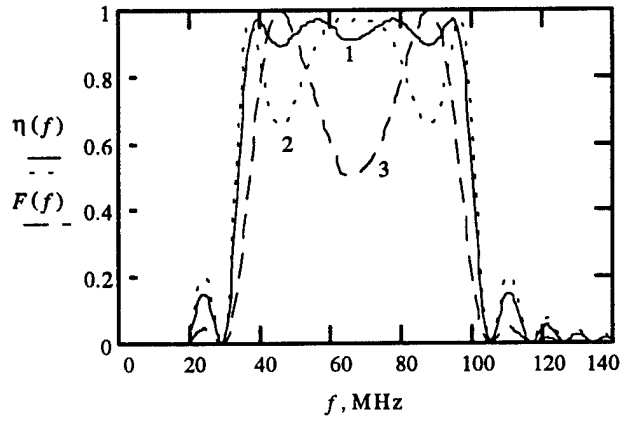

(b)

Fig. 3. Frequency characteristics of the 6° deflector at different P_a.

L=3 mm, H=6 mm, α_N=6°, θ_1=4.353°. (a) P_a=450 mW, Δf=59.6 MHz, N=550; (b) P_a=800 mW (curve 1), P_a=1100 mW (curve 2).

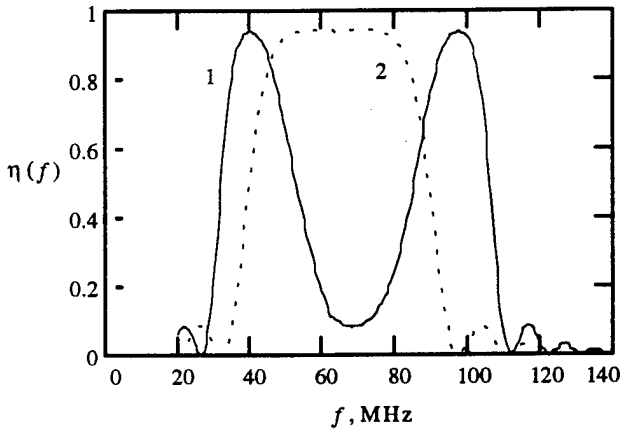

Fig. 4. Bifurcation (curve 1) and narrowing (curve 2) of frequency characteristic.

L=3 mm, H=6 mm, α_N=6°; P_a=450 mW. (1) θ_1=4.300°, Δf=80.9 MHz, N=744 (η_M<0.1). (2) θ_1=4.408°, Δf=21.3 MHz, N=197.

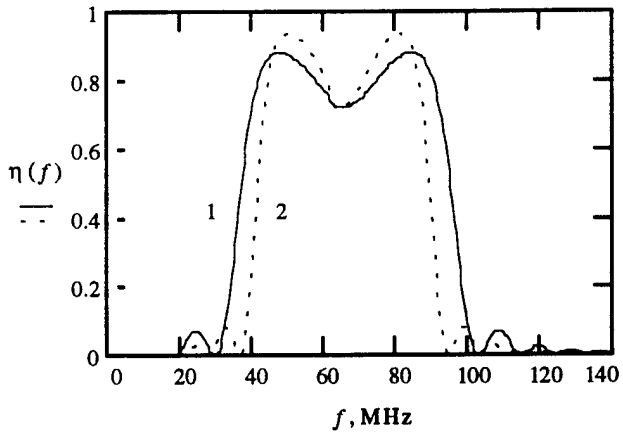

Fig. 5. Frequency characteristics of the 6° deflector at different constructive parameters.

(1) L=3 mm, H=6.5 mm, θ_1=4.368°; P_a=400 mW, η_M=0.722, N=522, Δf=52.1 MHz, f_{tr}=61.0, Δf_{tr}=86 %. (2) L=5 mm, H=8 mm, θ_1=4.382°; P_a=350 mW, η_M=0.720, N=543, Δf=44.1 MHz, f_{tr}=61.9, Δf_{tr} = 71 %.

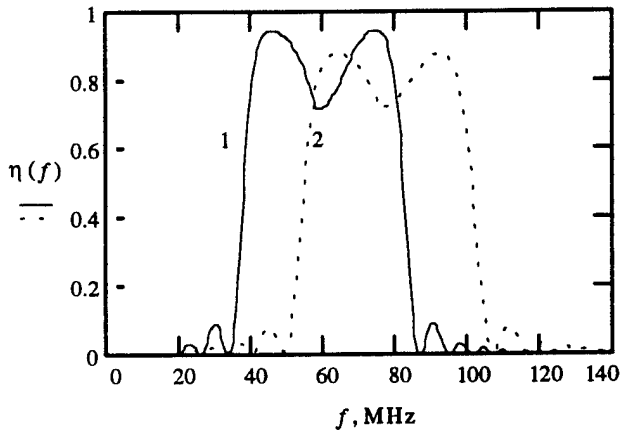

Fig. 6. Frequency characteristics of the 5.5° deflector at different wavelength. L=6 mm, H=8 mm, α_N=5.5°. (1) λ=633 nm, P_a=320 mW, θ_1=4.004°; η_M=0.716, N=512, Δf=41.2 MHz, f_{tr}=56.7 MHz, Δf_{tr}=73 %. (2) λ=514 nm, P_a=180mW, θ_1=3.963°; η_M=0.715, N=519, Δf=41.7 MHz, f_{tr}=75.5 MHz, Δf_{tr}=55 %.

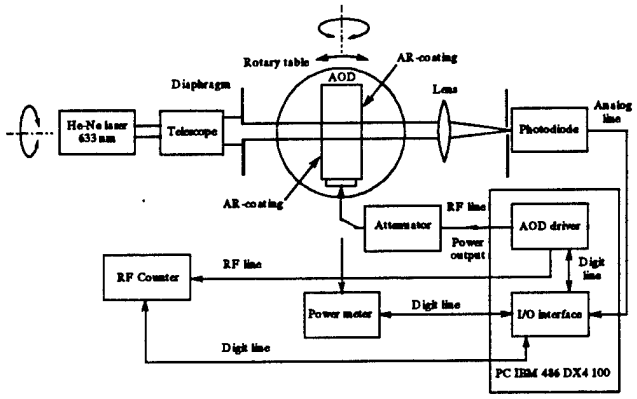

Fig. 7 Experimental setup for measuring frequency dependence of deflected light intensity.

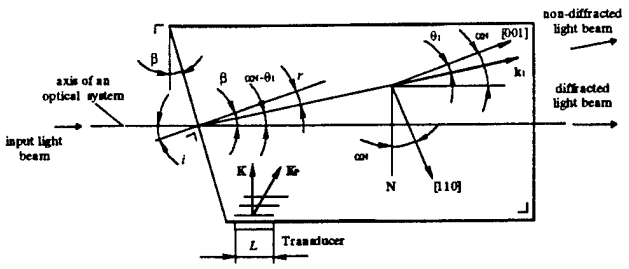

Fig. 8. Construction of Bragg cell for 2-D deflector.

$\mathbf{k}_1$ - wave vector of incident light; **K** - wave vector of sound; $\mathbf{K}_P$ - Poynting`s vector of sound; N - normal to the transducer.

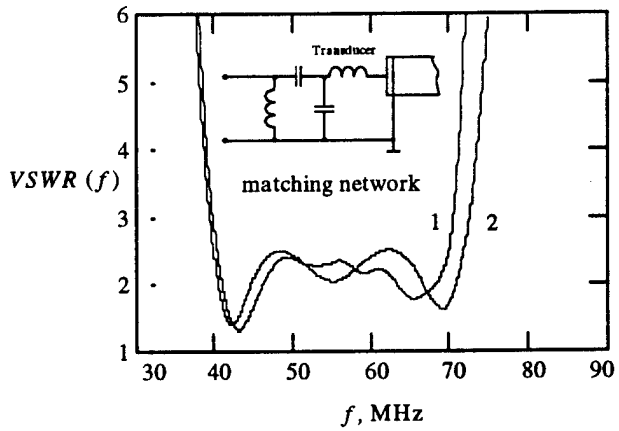

Fig. 9 Frequency dependencies of the input *VSWR* of the 5.5° deflector with an optimal matching network (1 - calculated, 2 - measured).

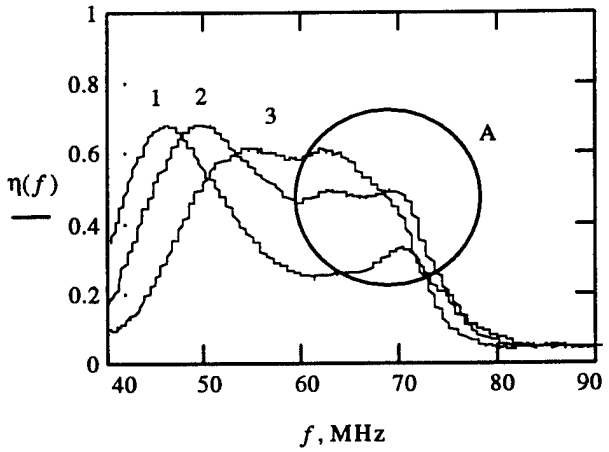

Fig. 10 Dependence of the 5.5° deflector frequency characteristic on the adjustment angle θ_{adj}.

P_{dr}=400 mW; $\theta_{adj}=\theta_{adj0}-3'$ (1); $\theta_{adj}=\theta_{adj0}$ (2); $\theta_{adj}=\theta_{adj0}+3'$ (3).

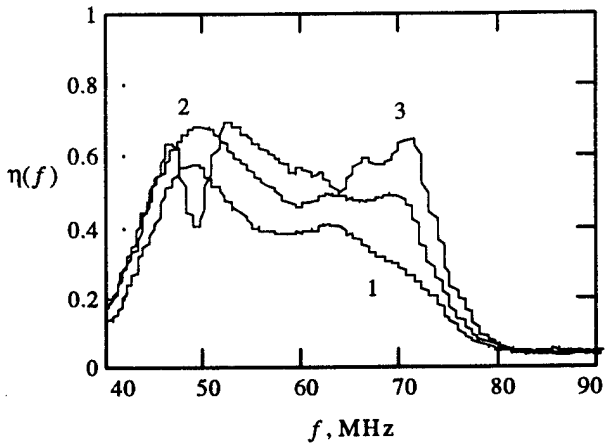

Fig. 11 Dependence of the 5.5° deflector frequency characteristic on the drive power P_{dr}.

$\theta_{adj}=\theta_{adj0}$; P_{dr} = 200 mW (1); P_{dr} = 400 mW (2); P_{dr} = 600 mW (3).

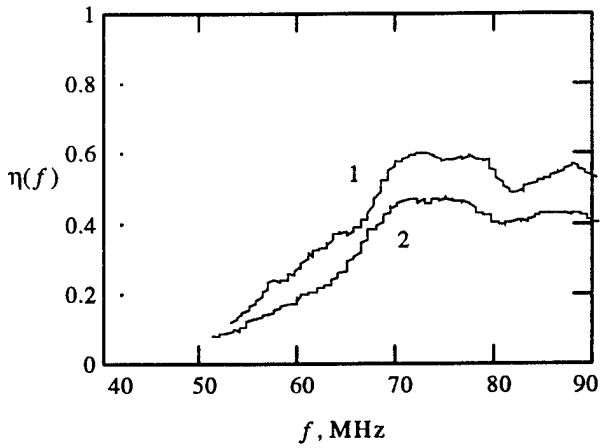

Fig. 12 Dependence of the 7.9° deflector frequency characteristic on the drive power P_{dr}.

P_{dr} = 800 mW (1); P_{dr} = 400 mW (2).

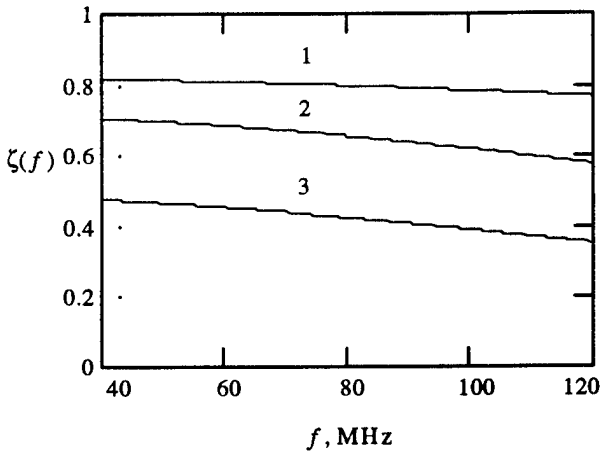

Fig. 13 Normalized intensity vs frequency of light diffracted under Bragg angle at different constructive parameters and drive power. α_N=6°, P_a=300 mW, L=3 mm, H=3 mm (1); α_N=5.5°, P_a=320 mW, L=6 mm, H=8 mm (2); α_N=7.9°, P_a=700 mW, L=2 mm, H=10 mm (3).

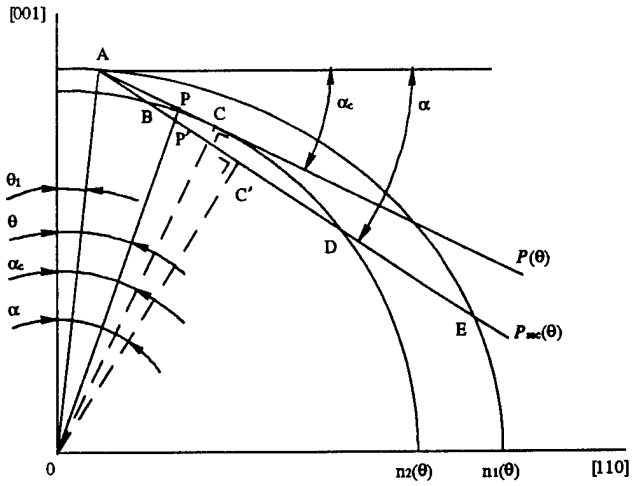

Fig. A1. The diagram for calculating of the numerical functions $\alpha_C(\theta_1)$ and $f_C(\theta_1)$ and $\alpha(f)$.